Conference papers

https://doi.org/10.52825/pv-symposium.v2i.2653

© Authors. This work is licensed under a Creative Commons Attribution 4.0 International License

Published: 13 Oct. 2025

# **Control for a Substring MPP Tracker**

Patrick Mader<sup>1</sup>, Sascha Eckerter<sup>1</sup>, Sebastian Coenen<sup>1</sup>, and Rainer Merz<sup>1</sup>

<sup>1</sup>University of Applied Sciences Karlsruhe, Germany

**Abstract.** A substring maximum power point (MPP) tracker is a power electronic circuit that increases the yield of partially shaded photovoltaic (PV) modules. It is integrated into the junction box of a PV module. During shading, a substring MPP tracker prevents bypass diodes from conducting and enables higher power extraction at the substring level. Instead of true substring MPP tracking, this approach focuses on balancing the substring voltages, as the MPP voltage is approximately independent of irradiation. The previous control method of the power electronics is based on voltage control of the substring voltages and current adjustment using MPP tracking. Parasitic effects lead to deviations from the actual MPP voltages under different shading conditions. This report therefore presents a new feedback-based control method for a substring MPP tracker. This method combines voltage control with feedback from the substring voltages and current adjustment using MPP tracking. Measurements at a laboratory-scale test setup demonstrate the functionality of the voltage control. Under partial shading conditions in the test setup, the feedback-based voltage control increases output power by up to 2.59% compared to the previous voltage control.

**Keywords:** PV Systems, Module Optimizer, Maximum Power Point, Substring MPP Tracking, Voltage Mode Control

#### 1. Introduction

Figure 1 shows the presented substring maximum power point (MPP) tracker [1][2][3]. It is suitable for direct installation in a module junction box and is parallel to the bypass diodes D1, D2, and D3 and the substrings S1, S2, and S3. A substring MPP tracker prevents the bypass diodes D1, D2, and D3 from conducting. It thus increases the output power  $P_{\rm out} = v_{\rm out} \cdot i_{\rm out}$  in the event of inhomogeneous irradiation [4]. The circuit consists of the DC-DC converters X1, X2, and X3, all implemented as buck converters [3]. The substring MPP tracker does not require any changes to the internal circuitry of the photovoltaic (PV) module [5][6] and does not require galvanic isolation [7]. Pulse-width modulated (PWM) signals PWM1, PWM2, and PWM3 with duty cycles  $d_1, d_2$ , and  $d_3$  control the DC-DC converters. The transmission behavior of the DC-DC converters results in the voltages [3]

$$v_1 = d_1 v_0, \tag{1}$$

$$v_2 = v_0 - v_1 - v_3 , (2)$$

$$v_3 = d_2 v_0$$
, (3)

$$v_{\text{out}} = d_3 v_0. \tag{4}$$

This allows for setting the three substring voltages  $v_1, v_2$ , and  $v_3$  using the duty cycles  $d_1, d_2$ , and  $d_3$ . Since the MPP voltages  $V_{1,\text{MPP}}, V_{2,\text{MPP}}$ , and  $V_{3,\text{MPP}}$  of the substrings S1, S2, and S3 remain approximately the same for different irradiances  $\Phi_1, \Phi_2$ , and  $\Phi_3$  and  $V_{1,\text{MPP}} \approx V_{2,\text{MPP}} \approx V_{3,\text{MPP}}$  applies [1][3], the previous control concept sets  $v_1 = v_2 = v_3$  with a voltage control without feedback. The duty cycles required for the DC-DC converters X1 and X2 are  $d_1 = d_2 = 1/3$  [3]. The DC-DC converters X1 and X2 thus form a voltage balancer for the substring voltages  $v_1, v_2$ , and  $v_3$ . The DC-DC converter X3 regulates the module current  $i_0$  to align with the higher string current  $i_{\text{out}}$ . In order to extract the maximum power  $P_{\text{out}}$  from the PV module, a classic MPP tracking algorithm such as the perturb-and-observe method [8] sets the duty cycle  $d_3$  so that  $v_1 \approx V_{1,\text{MPP}}$ ,  $v_2 \approx V_{2,\text{MPP}}$ , and  $v_3 = V_{3,\text{MPP}}$ .

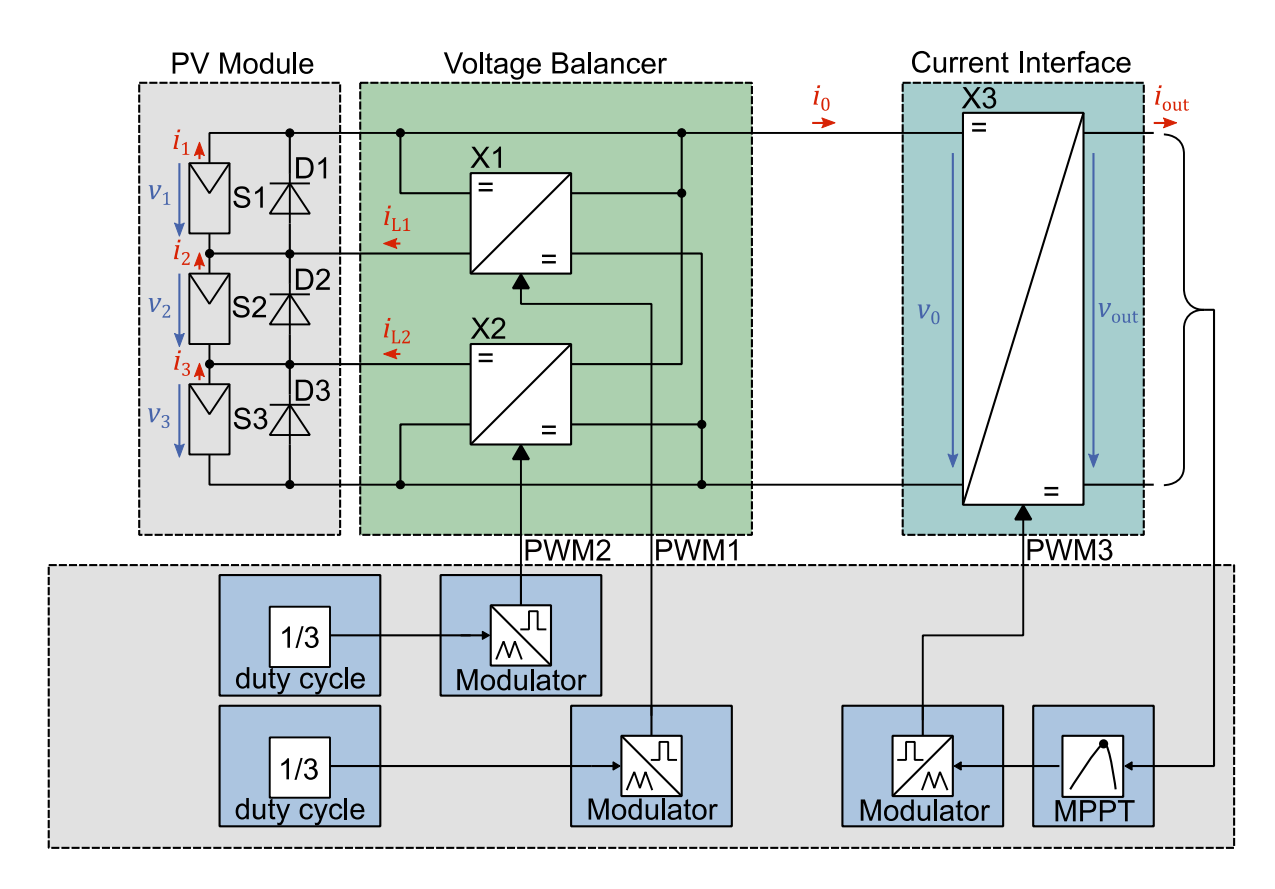


**Figure 1.** Block diagram of a substring MPP tracker. It is directly connected to a PV module with the three bypass diodes D1, D2, and D3. The substring MPP tracker consists of the three DC-DC converters X1, X2, and X3. The control concept uses an MPP tracker for the DC-DC converter X3 and a voltage control for DC-DC converters X1 and X2. Fixed control values lead to the same substring voltages  $v_1, v_2$ , and  $v_3$ , while neglecting parasitic effects.

Figure 2 shows measurements of the substring voltages  $v_1, v_2$ , and  $v_3$  of the existing control concept with the fixed duty cycles  $d_1=d_2=1/3$ . At the laboratory-scale test setup, laboratory power supplies with distinct source voltages  $V_{\rm S1}, V_{\rm S2}$ , and  $V_{\rm S3}$  along with series resistances  $R_1, R_2$ , and  $R_3$  constitute linear voltage sources. These voltage sources replace the substrings S1, S2, and S3 of the PV module, ensuring reproducible measurements. A linear voltage source with source voltage  $V_{\rm S1}=21\,\rm V$  and series resistance  $R_1=3\,\Omega$  replaces substring S1, a linear voltage source with source voltage  $V_{\rm S2}=21\,\rm V$  and series resistance  $R_2=7\,\Omega$  replaces substring S2, and a linear voltage source with source voltage  $V_{\rm S3}=21\,\rm V$  and series resistance  $R_3=3\,\Omega$  replaces substring S3. During measurements with shaded substrings, different substring voltages  $v_1, v_2$ , and  $v_3$  are obtained. The reasons for this are parasitic effects, such as non-ideal switches and component tolerances. Therefore, this report presents a new control concept based on voltage regulation for the voltages  $v_1, v_2$ , and  $v_3$ .

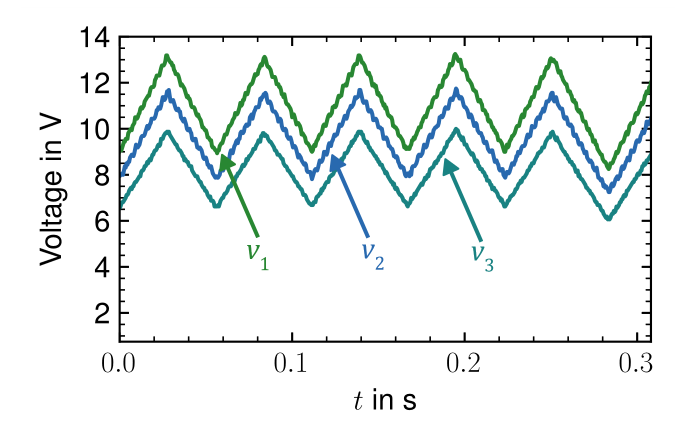


**Figure 2.** Results of the measurement of the three substring voltages  $v_1, v_2$ , and  $v_3$  with the implemented substring MPP tracker and voltage control without feedback on linear sources. Parasitic effects lead to unequal substring voltages  $v_1 \neq v_2 \neq v_3$ .

### 2. Feedback-based voltage control

Figure 3 shows the developed controller structure for the voltage balancer. The controller structure replaces the previous voltage control with  $d_1=d_2=1$  / 3 with a closed control loop for  $v_1=v_2=v_3$ .

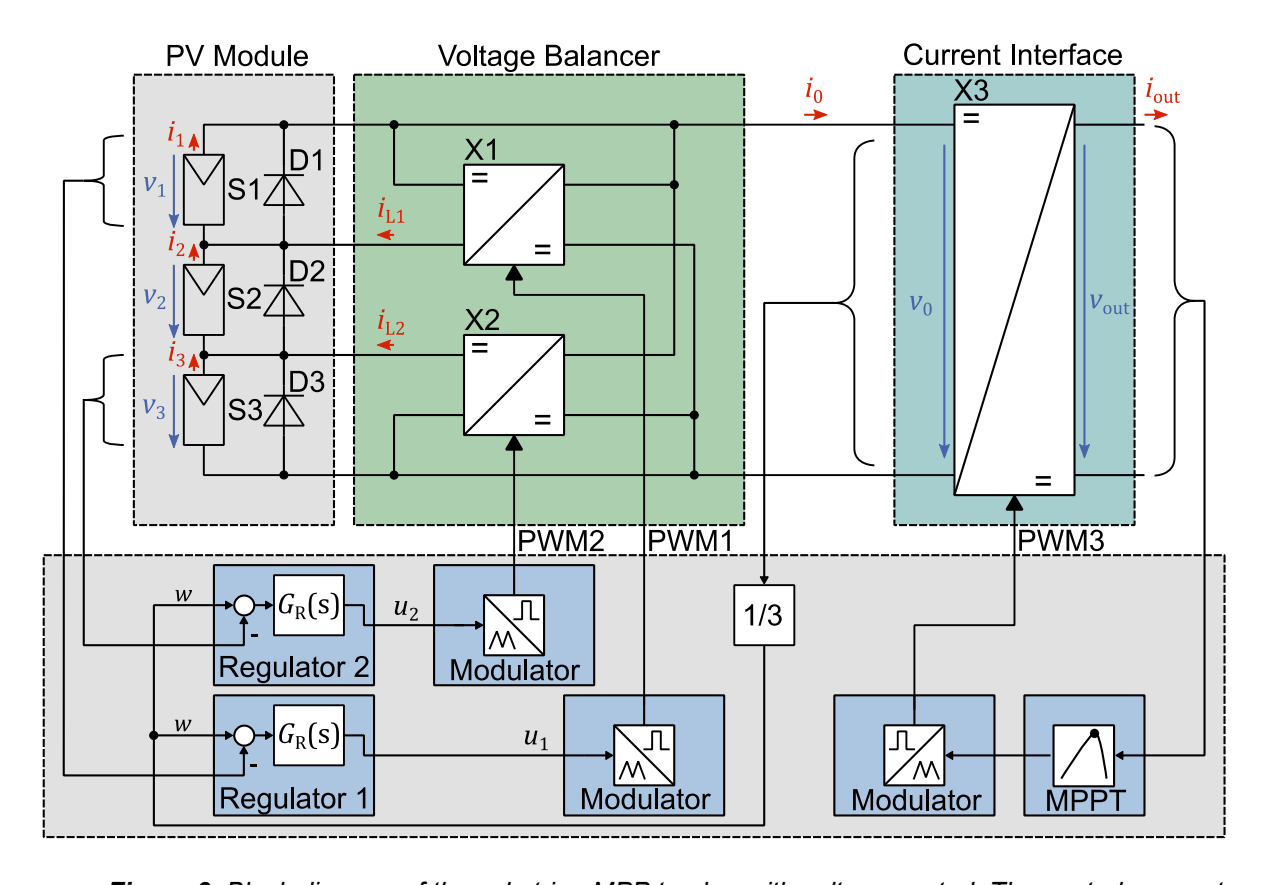


**Figure 3.** Block diagram of the substring MPP tracker with voltage control. The control concept uses an MPP tracker for the DC-DC converter X3 and voltage controls for the DC-DC converters X1 and X2. A measurement of the DC link voltage  $v_0$  results in the setpoint  $w=v_0$ /3 for the voltage controls. The actual variable for regulator 1 is the substring voltage  $v_1$  and the actual variable for regulator 2 is the substring voltage  $v_3$ . As a result, the control leads to equal substring voltages

$$v_1 = v_2 = v_3.$$

The closed control loop uses measurements of the substring voltages  $v_1$  and  $v_3$  as feedback and enables the compensation of parasitic effects that lead to unequal substring voltages  $v_1 \neq v_2 \neq v_3$ . The control system consists of regulator 1 and regulator 2, both of which have the transfer function  $G_{\rm FB}(s)$ . The setpoint  $w=v_0$  / 3 of the regulators is obtained from a measurement of the DC link voltage  $v_0$ . Furthermore, regulator 1 uses the substring voltage  $v_1$  as the actual value, and regulator 2 uses the substring voltage  $v_3$  as the actual value. Using the setpoint  $w=v_0$  / 3, regulator 1 regulates the substring voltage  $v_1=v_0$  / 3 and regulator 2 uses the setpoint  $w=v_0$  / 3 for the substring voltage  $v_3=v_0$  / 3. Kirchhoff's Voltage Law  $v_0=v_1+v_2+v_3$  therefore also results in  $v_2=v_0$ /3 and all substring voltages are the same.

### 2.1 Model of the plant

The basis for regulator synthesis is the modeling of the voltage balancer. Figure 4 shows the small-signal equivalent circuit of the voltage balancer. The modeling uses the small-signal equivalent circuit to derive the mathematical relationships between the substring voltages  $v_1$ ,  $v_2$ , and  $v_3$  and the duty cycles  $d_1$  and  $d_2$ .

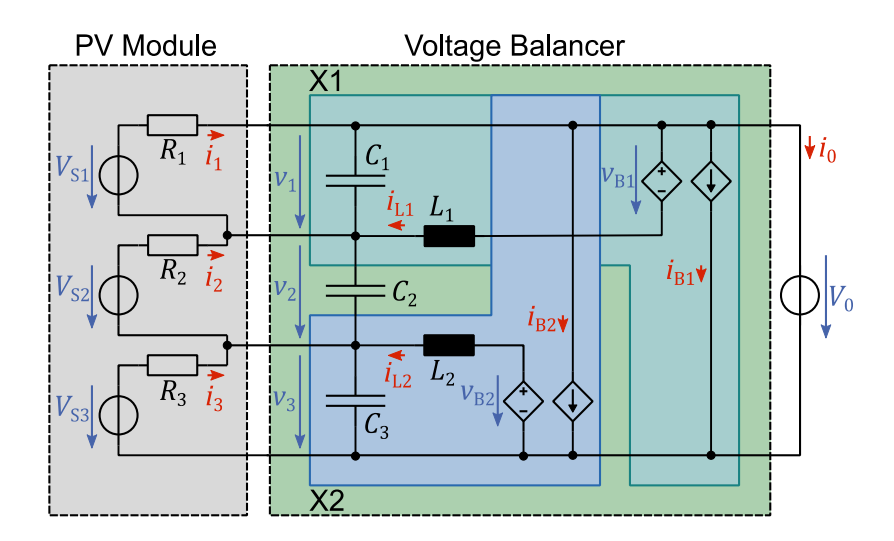


**Figure 4.** Small-signal equivalent circuit of the voltage balancer. Linear voltage sources with the voltage sources  $V_{S1}$  to  $V_{S3}$  and internal resistances  $R_1$  to  $R_3$  replace the non-linear characteristics of the substrings S1, S2, and S3. Linear voltage sources  $v_{B1}$  and  $v_{B2}$  and linear current sources  $i_{B1}$  and  $i_{B2}$  replace the half-bridges of the buck converters X1 and X2.

With small-signal behavior, it is possible to approximate the non-linear current-voltage characteristic of the substrings S1, S2, and S3 using linear voltage sources  $V_{\rm S1}$  to  $V_{\rm S3}$  with the internal resistances  $R_1$  to  $R_3$ . At the operating point of the control loop, the substrings operate at the MPP and the module supplies the MPP voltage  $V_{\rm MPP}$  and the MPP current  $I_{\rm MPP}$ . The values of the components can be calculated using the impedance matching principle. This results in the source voltages  $V_{\rm Sx}=2/3\,V_{\rm MPP}$  and the internal resistances  $R_x=V_{\rm MPP}/(3I_{\rm MPP})$ , with  $x\in[1,2,3]$ . The two buck converters X1 and X2 can also be simplified using linearized models. The buck converter X1 consists of the voltage source  $v_{\rm B1}=d_1v_{\rm O}$ , the current source  $i_{\rm B1}=d_1i_{\rm L1}$  and the inductance  $L_1$  and the buck converter X2 consists of the voltage source  $v_{\rm B2}=d_2v_{\rm O}$ , the current source  $i_{\rm B2}=d_2i_{\rm L1}$  and the inductance  $L_2$ . The DC link voltage  $V_{\rm O}$  and the voltage sources  $V_{\rm S1}$  to  $V_{\rm S3}$  are simplified in small-signal behavior by a short circuit, as they are assumed to be constant. This results in the transfer functions

$$G_{11}(s) := \frac{v_1(s)}{V_0 d_1(s)} = \frac{2CLs^2 + \frac{2L}{R}s + 1}{3C^2 L^2 s^4 + \frac{6CL^2}{R}s^3 + \left(4CL + \frac{3L^2}{R^2}\right)s^2 + \frac{4L}{R}s + 1},\tag{5}$$

$$G_{31}(s) := \frac{v_3(s)}{V_0 d_1(s)} = \frac{-CLs^2 - \frac{L}{R}s}{3C^2 L^2 s^4 + \frac{6CL^2}{R}s^3 + \left(4CL + \frac{3L^2}{R^2}\right)s^2 + \frac{4L}{R}s + 1}$$
 (6)

for the duty cycle  $d_1$ . Due to the symmetry of the circuit, the transfer functions

$$G_{12}(s) := \frac{v_1(s)}{V_0 d_2(s)} \equiv G_{31}(s),$$
 (7)

$$G_{32}(s) := \frac{v_3(s)}{V_0 d_2(s)} \equiv G_{11}(s)$$
 (8)

for duty cycle  $d_2$ , are similar to transfer functions with  $d_1$ . Furthermore, due to the symmetries, both substring voltages  $v_1$  and  $v_3$  can be controlled with the same controller structure.

### 2.2 Controller design

Since the controller designs of regulator 1 and regulator 2 are identical, the following section focuses solely on the controller design for regulator 1. Figure 5 shows the closed control loop of the voltage control.

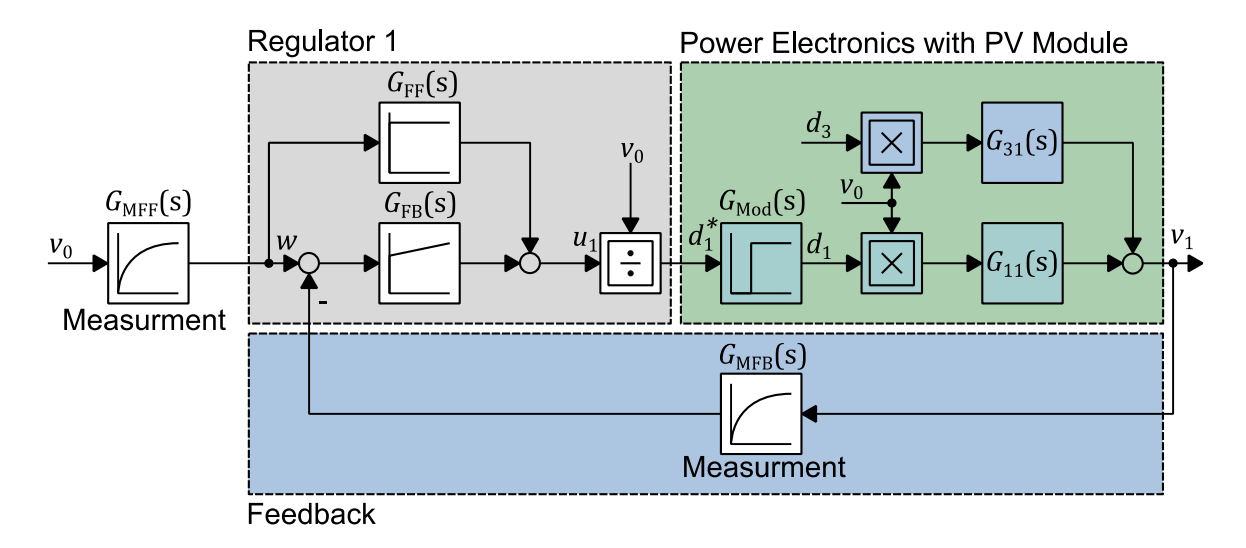


**Figure 5.** Closed control loop of the substring voltage  $v_1$ . Transfer functions  $G_{11}(s)$  and  $G_{31}(s)$  describe the power electronics with a PV module. Transfer function  $G_{Mod}(s)$  describes the modulation. Filters  $G_{MFF}(s)$  and  $G_{MFB}(s)$  prevent aliasing. Controller structure consists of a PI controller  $G_{FB}(s)$ , a feedforward control  $G_{FF}(s)$  and the division  $d_1^* = u_1/v_0$ .

In the output variable  $v_1 = G_{11}(s)V_0d_1 + G_{31}(s)V_0d_2$ , the manipulated variable  $d_3$  of the other substring voltage  $v_3$  occurs as a disturbance variable in the control loop for  $v_1$ . Furthermore, the control loop consists of the transfer function

$$G_{\text{Mod}}(s) = e^{-sT_{\text{t}}} \approx \frac{1}{1 + sT_{\text{t}}}$$
(9)

of the modulator with the dead time  $T_{\rm t}$ . In time average, the dead time  $T_{\rm t}=T_{\rm PWM}/2$  is half the switching period  $T_{\rm PWM}$ . The measurement of the set value  $V_0$  and the actual variable  $v_1$  uses the anti-aliasing filters

$$G_{\rm MFF}(s) = \frac{k_{\rm M}}{1 + sT_{\rm M}} \tag{10}$$

and

$$G_{\text{MFB}}(s) = 3G_{\text{MFF}}(s), \tag{11}$$

with the gain  $k_{\rm M}$  and the time constant  $T_{\rm M}$ . The controller consists of a PI controller

$$G_{\rm FB}(s) = k_{\rm FB} \frac{1 + T_{\rm N}s}{T_{\rm N}s},$$
 (12)

with the gain  $k_{\rm FB}$  and the reset time  $T_{\rm N}$ , for the stationary, precise compensation of the parasitic effects. In addition, the controller structure has a feedforward control  $G_{\rm FF}(s)=1$  to improve the dynamics of the control. To compensate for the operating point-dependent gain of the controlled system from equation (5), the controller structure contains an additional division point  $d_1^*=u_1/V_0$ . The PI controller is set based on the frequency characteristic of the open control loop. Figure 6 shows the Bode diagram of the open control loop without controller

$$G_{0}(\omega) = G_{\text{Mod}}(\omega)G_{11}(\omega)G_{\text{MFB}}(\omega)$$
(13)

and the designed controller  $G_{\rm FB}(\omega)$ . The numerator time constant of the PI controller compensates for the system time constant  $T_{\rm N}=1/\omega_{11}$ . The selected gain  $k_{\rm FB}$  results in a phase margin at the crossing frequency  $\omega_{\rm D}$  of the open control loop of  $\varphi=45^{\circ}$ . This results in a good compromise between disturbance and command response.

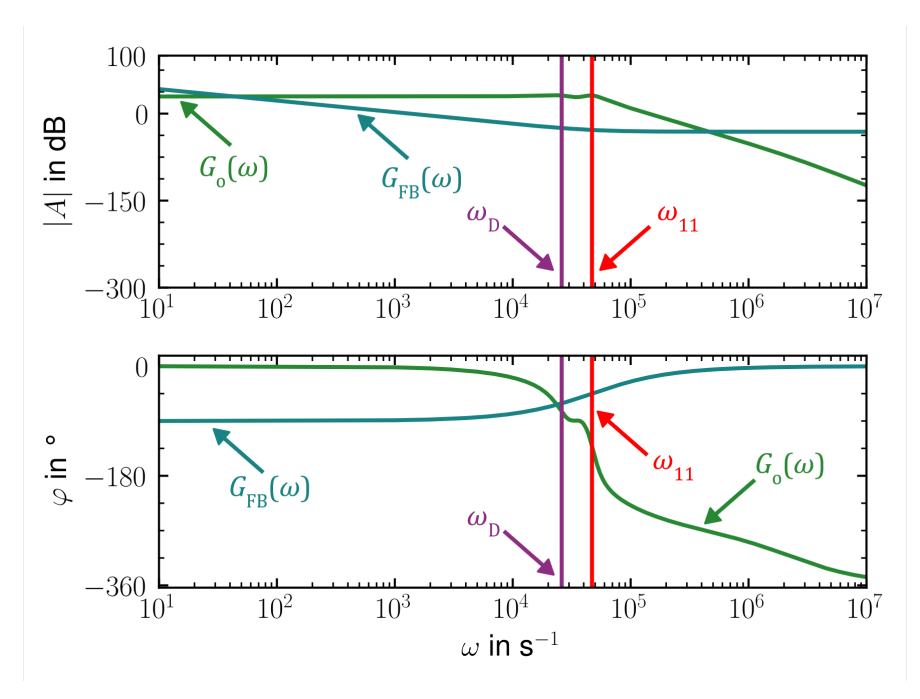


**Figure 6.** Bode diagram of the open control loop  $G_o(\omega)$  and the PI controller  $G_{FB}(\omega)$ . The Numerator time constant of the PI controller compensates for the system time constant  $\omega_{11}$  and controller gain  $k_{FB}$  leads to a phase margin of  $\varphi=45^\circ$ .

#### 3. Measurement

The measurements are divided into a measurement on linear sources to check the voltage regulation and a measurement on a PV module to determine the additional yield of the newly developed control structure.

### 3.1 Voltage measurement on linear sources

Figure 7 shows the measurement results of the substring voltages  $v_1, v_2$ , and  $v_3$  with the voltage regulation. The measurement setup with the feedback-based voltage control is identical to the measurement using the voltage control. A linear voltage source with source voltage  $V_{\rm S1}=21\,\rm V$  and series resistance  $R_1=3\,\Omega$  replaces the substring S1, a linear voltage source with source voltage  $V_{\rm S2}=21\,\rm V$  and series resistance  $R_2=7\,\Omega$  replaces the substring S2, and a linear voltage source with source voltage  $V_{\rm S3}=21\,\rm V$  and series resistance  $R_3=3\,\Omega$  replaces the substring S3. The substring voltages  $v_1,v_2$ , and  $v_3$  have an identical curve,  $v_1=v_2=v_3$ . The measurements prove the feedback-based voltage control.

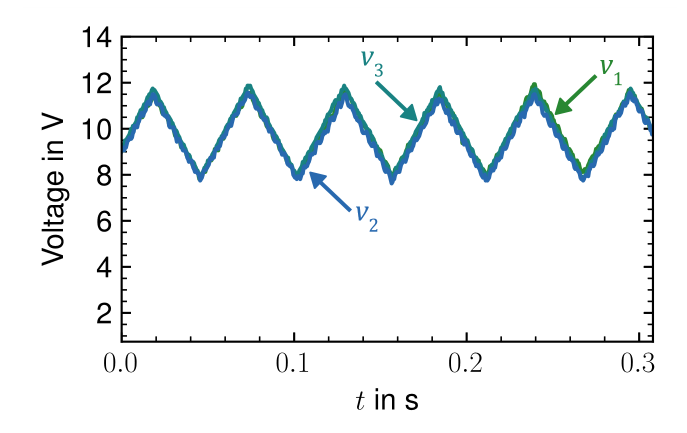


**Figure 7.** Results of the measurement of the substring voltages  $v_1, v_2$ , and  $v_3$  with the implemented substring MPP tracker and feedback-based voltage control on linear sources. The presented voltage control leads to equal substring voltages  $v_1 = v_2 = v_3$ .

#### 3.2 Yield measurements on a PV module

Figure 8 shows the measurement result of the newly developed method on a PV module. The additional yield is defined as

$$\varepsilon := \frac{P_{\text{out,rgr}}}{P_{\text{out,stg}}} - 1 \tag{14}$$

and indicates the ratio of output power of the feedback-based voltage control  $P_{\mathrm{out,rgr}}$  in relation to the output power  $P_{\mathrm{out,stg}}$  without feedback. In the measurement setup, an LED table illuminates a PV module, while artificial shading limits the irradiation on the substrings. The irradiation scenarios used only differ in the irradiation for substring S3, which is  $\varphi_3 := \Phi_3 / \Phi_N \in \{100\%, 75\%, 50\%, 25\%\}$ , based on the nominal irradiation  $\Phi_N$ . The two remaining substrings S1 and S2 remain constant at  $\varphi_1 := \Phi_2/\Phi_N = 100\%$ and  $\varphi_2 := \Phi_2 / \Phi_N = 100\%$ , also based on the nominal irradiation  $\Phi_N$ . The measurement results show the additional yield due to voltage control. With uniform irradiation  $\varphi_1 = 100\%$ ,  $\varphi_2 = 100\%$ , and  $\varphi_3 = 100\%$ , the additional yield compared to voltage control increases by  $\varepsilon=2.49\%$  and with very uneven irradiation  $\varphi_1=100\%, \varphi_2=100\%,$  and  $\varphi_3$  = 25%, the additional yield is  $\varepsilon$  = 2.59%. Even in the medium scenarios  $\varphi_1 = 100\%$ ,  $\varphi_2 = 100\%$ ,  $\varphi_3 = 75\%$  and  $\varphi_1 = 100\%$ ,  $\varphi_2 = 100\%$ ,  $\varphi_3 = 50\%$ , there are slight additional yields of  $\varepsilon=0.69\%$  and  $\varepsilon=0.57\%$ . The lower yield gain in medium scenarios  $\varphi_1=100\%$ ,  $\varphi_2=100\%$ ,  $\varphi_3=75\%$  and  $\varphi_1=100\%$ ,  $\varphi_2=100\%$ ,  $\varphi_3=50\%$ , is attributed to the slight dependence of the actual MPP voltage on irradiation. Under midrange irradiation conditions, the optimal MPP voltage is less precisely attained compared to other irradiation levels. Nevertheless, a yield increase can be observed across all irradiation scenarios.

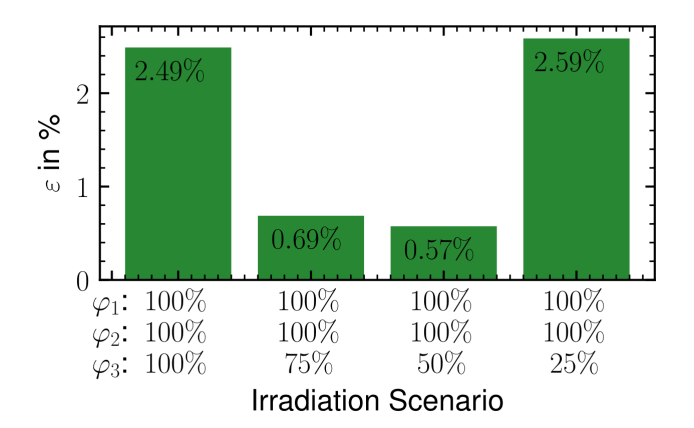


**Figure 8.** Percentage additional yield  $\varepsilon$  of the feedback-based voltage control compared to the voltage control without feedback when operating a PV module for different relative irradiances  $\varphi_1$ ,  $\varphi_2$ , and  $\varphi_3$ .

Additional yield occurs in all irradiance scenarios.

### 4. Summary

The substring MPP tracker consists of three nested DC-DC converters and enables the substrings of a PV module to operate at MPP even in the case of partial shading. The voltage at which a substring delivers maximum power is approximately independent of irradiation. Therefore, the previous control method of the substring MPP tracker is based on a control with the same duty cycle for the voltage balancer, which should lead to the same substring voltages. An MPP tracker controls the current interface so that all substrings operate at MPP. Measurements show that parasitic effects lead to different substring voltages depending on the shading scenario when controlled with the same duty cycles. This report therefore presented a new feedback-based voltage control for the two DC-DC converters of the voltage balancer. The setpoints of the controllers result from a measurement of the DC link voltage and lead to the same substring voltages, even in the case of parasitic effects. This report derives the circuit model required for the controller design and then shows the controller synthesis using the Bode diagram. The developed control method was successfully tested on test hardware with linear sources. The control leads to an even voltage distribution across the substrings. Furthermore, measurements on a PV module with a lighting table show additional yields through the control of up to 2.59% compared to voltage control in the selected irradiation scenarios.

# **Data availability statement**

The authors do not have permission to share data.

#### **Author contributions**

**Patrick Mader:** Conceptualization, Data curation, Formal analysis, Investigation, Methodology, Software, Validation, Visualization, Writing - original draft. **Sascha Eckerter:** Writing - review & editing. **Sebastian Coenen:** Writing - review & editing. **Rainer Merz:** Funding acquisition, Project administration, Supervision, Writing - review & editing.

# **Competing interests**

The authors declare that they have no competing interests.

### **Funding**

This work contributes to the research performed at the University of Applied Science Karlsruhe. The results were generated within the project "Solarpark 2.0" (funding code 03EE1135C) funded by the Federal Ministry for Economic Affairs and Climate Action (BMWK).

### **Acknowledgement**

The authors would like to thank the Federal Ministry for Economic Affairs and Climate for financing the development of the substring MPP tracker within the framework of the federal project Solarpark 2.0 with the number FKZ: 03EE1135C.

### References

- [1] R. Merz, S. Eckerter, S. Coenen und P. Mader. "Substring-MPPT steigert Strangleistung bei Teilverschattung". In Tagungsunterlagen 39. PV-Symposium 2024.
- [2] R. Brace, A. Neumann, T. Czarnecki und R. Merz "Substring-MPPT For 4-Terminal 3-Substring Modules". In 35th European Photovoltaic Solar Energy Conference and Exhibition, 2018, DOI: 10.4229/35thEUPVSEC20182018-5CV.3.57.
- [3] P. Mader, S. Eckerter, und R. Merz. "Design of the Substring MPP Tracker". In 41th European Photovoltaic Solar Energy Conference and Exhibition, 2024, DOI: 10.4229/EUPVSEC2024/3AV.1.40.
- [4] S. Eckerter, K. Kerekes, P. Mader und R. Merz, "Analysis of Irradiation Differences on Substringlevel in Solar Parks,". In 41th European Photovoltaic Solar Energy Conference and Exhibition, 2024, DOI: 10.4229/EUPVSEC2024/4DV.4.13.
- [5] "Maxim Integrated, "MAX20801 MPP Tracking DC-DC Converter," 2019. [Online]. Available: <a href="https://www.mouser.de/pdfDocs/MAX20801.pdf">https://www.mouser.de/pdfDocs/MAX20801.pdf</a>. [Zugriff am 2024].
- [6] B. Burger, B. Goeldi, S. Rogalla, H. Schmidt. "Module Integrated Electronics An Overview" In 25th European Photovoltaic Solar Energy Conference and Exhibition, 2010, DOI: 10.4229/25thEUPVSEC2010-4EP.1.1.
- [7] C. Schöner, G. Rouffaud, L. Probst und H. Schmidt. "Untersuchung einer galvanisch getrennten DC/DC-Topologie als Eingangsstufe eines PV-Modulwechselrichters mit Teilstringanbindung". In Tagungsunterlagen 34. PV-Symposium, 2019.
- [8] T. Suntio, T. Messo and J. Puukko. "Power Electronic Converters: Dynamics and Control in Conventional and Renewable Energy Applications". John Wiley & Sons, 2017, DOI: 10.1002/9783527698523.